

## Hyperthermal alkali-ion scattering from a metal surface: A theoretical study of the potential

P. J. van den Hoek, A. D. Tenner, and A. W. Kleyn

*FOM Institute for Atomic and Molecular Physics, Kruislaan 407, NL-1098 SJ Amsterdam, The Netherlands*

E. J. Baerends

*Department of Theoretical Chemistry, Free University of Amsterdam, De Boelelaan 1083, NL-1081 HV Amsterdam, The Netherlands*

(Received 6 May 1986)

The  $K^+$ -W ion-atom scattering potential is calculated with the Hartree-Fock-Slater linear combination of atomic orbitals (HFS-LCAO) method. For hyperthermal (10–100 eV)  $K^+$  scattering from a W(110) surface, classical-trajectory calculations are performed, where the  $K^+$ -W(110) ion-surface potential is represented by a sum of pairwise-calculated (HFS-LCAO)  $K^+$ -W potentials. The results of these classical-trajectory calculations are compared with experiment and with the results of similar trajectory calculations using a sum of Ziegler-Biersack-Littmarck “universal” pair potentials. From these comparisons, it turns out that the HFS-LCAO pair potential is able to reproduce well on-top-site hyperthermal  $K^+$  scattering from a W(110) surface, contrary to the Ziegler-Biersack-Littmarck potential, which clearly does not work very well in this low-energy range. The inability of the HFS-LCAO pair potential to give a proper description of  $K^+$  scattering from the hollow site of the W(110) surface unit cell can be ascribed to the breakdown of a summation of pair potentials. This is clear from the difference between the sum of the calculated  $K^+$ -W ion-atom potentials and a calculated  $K^+$ - $W_5$  ion-cluster potential, the cluster representing the W(110) surface. The ion-cluster calculations indicate an extra repulsion of about 10% at the center of the W(110) surface unit cell. This extra hollow-site repulsion can be explained by analyzing the properties of the exchange (Pauli, Born) repulsions between the  $K^+$  ion and (i) one W atom and (ii) the W(110) surface ( $W_5$  cluster) at the hollow site.

### I. INTRODUCTION

The interaction of a surface with an incoming particle can be viewed in two different ways. At high incident energies ( $E > 1$  keV), the particle only “sees” the individual surface atoms. Therefore, scattering from a surface at these energies is represented very well by sequences of binary collisions with the atomic cores.<sup>1</sup> At low energies ( $E < 1$  eV), on the other hand, the particle sees the surface as a whole. Here, no scattering from individual atoms takes place, but from a corrugated surface.<sup>2</sup> Between these two extrema there is a large energy range where the interaction will be represented by some mixture of both descriptions.

In order to gain insight into the particle-surface potential in the hyperthermal energy range, Tenner *et al.* performed experiments on  $K^+$  scattering at normal incidence from a W(110) surface for incident energies between 10 and 100 eV.<sup>3</sup> They measured for the first time both the angular and final energy dependence of the scattered  $K^+$ -ion intensity. The data were analyzed by classical-trajectory calculations using an *ad hoc* model potential given by the sum of pairwise Born-Mayer (BM) repulsive terms and an attractive image potential. That is, the ion-surface potential  $V(x,y,z)$  was decomposed as follows:<sup>4</sup>

$$V = \sum_i U(|\mathbf{r} - \mathbf{R}_i|) + S \sum_j U(|\mathbf{r} - \mathbf{R}_j|) + V_{\text{im}}, \quad (1a)$$

with

$$U(r) = Ae^{-\rho r} \quad (1b)$$

and

$$V_{\text{im}}(z) = \begin{cases} -\frac{e^2}{[(z - z_0)^2 + z_m^2]^{1/2}}, & z > z_0 \\ -\frac{e^2}{4z_m}, & z \leq z_0. \end{cases} \quad (1c)$$

In Eq. (1) the  $z$  direction is defined to be normal to the surface;  $\mathbf{R}_i$  and  $\mathbf{R}_j$  are the positions of first- and second-layer tungsten atoms  $i$  and  $j$ , respectively. The image potential  $V_{\text{im}}$  [Eq. (1c)] is small compared to the repulsive potentials  $U$  in the energy range under consideration (10–100 eV).<sup>4</sup> A comparison between experimental results and simulations indicated the presence of an extra repulsion at the hollow site of the surface unit cell, which was accounted for by putting  $S=12$  in Eq. (1a). The other parameters  $A$ ,  $\rho$ ,  $z_0$ , and  $z_m$  were determined by a best fit to the experimental data for incident energy  $E_0=35$  eV [see Figs. 4(a) and 4(b)].

Other model potentials may be used to represent the  $K^+$ -W(110) interaction. The parameters appearing in Eq. (1) may be modified, depending on the range of the incident energy  $E_0$ .<sup>5,6</sup> Hulpke and Mann<sup>6</sup> accounted for the additional hollow-site repulsion by adding an extra  $z$ -dependent term. However, simulations with both the potential of Hurkmans<sup>5</sup> and that of Hulpke showed no resemblance at all to the experimental data of Tenner *et al.*<sup>4</sup>

Another possibility, using  $S=1$ , is to take for  $U(r)$  the

Ziegler-Biersack-Littmark (ZBL) "universal" potential, which has been determined on the basis of free-electron gas (FEG) calculations.<sup>7</sup> For the  $K^+$ -W system, this potential is given by<sup>4</sup>

$$U(r) = \frac{20246}{r} (0.28022e^{-4.008r} + 0.028171e^{-2.006r}), \quad (2)$$

where length and potential energy are defined in units of Å and eV, respectively. Simulations using this potential yield intensity spectra which show a certain, although unsatisfactory, resemblance with Tenner's experimental results<sup>4</sup> [Fig. 4(d)]. At higher energies ( $\geq 250$  eV), however, the ZBL potential has been found to work very well for scattering of  $Li^+$ ,  $Na^+$ , and  $K^+$  from  $Mo(001)$ .<sup>8</sup>

The three mentioned approaches<sup>4-6</sup> of the  $K^+$ -W(110) ion-surface interaction have in common that they use a simple model potential of which a number of parameters is varied so as to give the best agreement with experiment. It would be interesting, however, to learn something about the nature of the ion-surface potential from a more theoretical point of view. It is the scope of this work to perform potential energy calculations from first principles, the results of which can directly be compared with experiment. More specifically, we present a  $K^+$ -W ion-atom potential which can be used within the "pairwise approximation." Furthermore, our calculations provide direct evidence for extra repulsion with respect to a summation of pair potentials at the center of the W(110) surface unit cell and give some insight into the mechanisms leading to this repulsion.

$K^+$ -W(110) ion-surface potentials were calculated for a  $K^+$  ion approaching on the top site and on the hollow site of the surface unit cell. In these calculations, the surface was approximated by a cluster of five W atoms. The validity of representing a surface by finite (often small) clusters has been thoroughly discussed by, e.g., Post and Baerends.<sup>9</sup> The clear advantage of this approach is the possibility to use well-established quantum-chemical methods. As for alkali-atom scattering at energies around 50 eV, it has been argued that since the duration of the scattering event is very short [ $10^{-13}$  s (Ref. 4)], the atom-surface interaction may be assumed localized within the region of a few surface atoms.<sup>10</sup> For ions, however, there remains the problem of the (long-range) image charge formation. We will discuss this in some more detail in Sec. III. Within the cluster approach, we are able to solve the many-electron problem with only a very limited number of approximations. Therefore, our calculations can serve as a benchmark for other calculations with only a small number of surface atoms using more approximate schemes.<sup>10-12</sup>

In Sec. II of this paper we will briefly outline the computational method. In Sec. III results are presented and discussed. The conclusions are summarized in Sec. IV.

## II. METHOD

The calculations have been performed using a Hartree-Fock-Slater (HFS) LCAO program package.<sup>13</sup> The

Hartree-Fock-Slater method is characterized by a local  $X\alpha$  exchange potential, in which it differs from the Hartree-Fock method. In all calculations, we put  $\alpha=0.7$ .<sup>13</sup> A recently developed numerical integration scheme<sup>14</sup> allowed for the accurate and efficient evaluation of matrix elements appearing in the secular equation. We used a standard Slater-type orbital STO basis set,<sup>15</sup> together with a  $6p$  polarization function, for the tungsten atom. For the potassium ion basis functions were separately optimized. Table I gives a complete list of the basis functions used. As a test of their quality, HFS-LCAO one-electron energies for the tungsten atom and potassium ion are compared with numerical values resulting from Herman-Skillman-type atomic calculations.

The interaction energy between the atoms (fragments) of a molecule was calculated using Ziegler's transition state method,<sup>16</sup> which circumvents errors due to subtracting two large total energy values. The expression for the interaction energy  $\Delta E$  is

$$\Delta E = \Delta E_{el} + \Delta E_X + \Delta E_{TS}, \quad (3a)$$

TABLE I. Basis functions (Slater-type orbitals) and orbital energies for atoms.

Basis functions			
Type	W Exponent ( $a_0^{-1}$ )	Type	K <sup>+</sup> Exponent ( $a_0^{-1}$ )
1s <sup>a</sup>	48.00	1s <sup>a</sup>	15.09
2s <sup>a</sup>	28.40	2s <sup>a</sup>	6.50
3s <sup>a</sup>	16.55	2p <sup>a</sup>	7.74
4s <sup>a</sup>	11.30	3s	2.41
5s <sup>a</sup>	5.40	3s'	3.69
2p <sup>a</sup>	33.76	3p	1.80
3p <sup>a</sup>	17.59	3p'	3.01
4p <sup>a</sup>	9.40	4s	0.84
5p <sup>a</sup>	4.13	4s'	1.30
3d <sup>a</sup>	21.00	4s''	2.08
4d <sup>a</sup>	10.10		
4f <sup>a</sup>	6.49		
5d	1.30		
5d'	2.35		
5d''	4.20		
6s	1.00		
6s'	1.55		
6s''	2.50		
6p	2.00		
Orbital energies (eV)			
W		K <sup>+</sup>	
Numerical atomic calculations (Herman-Skillman)			
$\epsilon_{5d}$	-5.20	$\epsilon_{3s}$	-40.14
$\epsilon_{6s}$	-4.19	$\epsilon_{3p}$	-24.05
		$\epsilon_{4s}$	-5.61
Hartree-Fock-Slater calculation			
$\epsilon_{5d}$	-5.20	$\epsilon_{3s}$	-40.22
$\epsilon_{6s}$	-4.19	$\epsilon_{3p}$	-24.08
		$\epsilon_{4s}$	-5.61

<sup>a</sup>Added for core orthogonalization.

where  $\Delta E_{el}$  is the (classical) Coulomb attraction between the atoms (fragments), and  $\Delta E_X$  and  $\Delta E_{TS}$  are given by

$$\Delta E_X = \frac{3}{4} \int \left[ \rho V_{X\alpha}(\rho) - \sum_A \rho_A V_{X\alpha}(\rho_A) \right] d\tau, \quad (3b)$$

$$\Delta E_{TS} = \sum_{i,j} \Delta P_{ij} \left[ \frac{1}{6} F_{ij}(\rho) + \frac{2}{3} F_{ij} \left[ \frac{\rho + \bar{\rho}}{2} \right] + \frac{1}{6} F_{ij}(\bar{\rho}) \right]. \quad (3c)$$

The sum in Eq. (3b) ranges over all atoms (fragments)  $A$ ; the electron density  $\rho$  is the sum of the atomic (fragment) electron densities,  $\rho = \sum_A \rho_A$ . The population matrix  $\Delta P$  in Eq. (3c) describes the change in going from  $\rho$  to the fully converged molecular self-consistent-field (SCF) density  $\bar{\rho}$ . The  $F_{ij}$  are the elements of the Fock matrix, which depends, of course, on the electron density. Equation (3) is exact to fourth order in  $\Delta P$ .

If we use in Eq. (3c) instead of the converged molecular density  $\bar{\rho}$ , the density  $\rho^0$  which is obtained from the antisymmetrized product of atomic (fragment) wave functions, we obtain the exchange repulsion  $\Delta E^0 (= \Delta E_{el} + \Delta E_X + \Delta E_{TS}^0)$  between the atoms (fragments) of the molecule. For a further discussion on exchange repulsion, see Sec. III E.

### III. RESULTS AND DISCUSSION

#### A. $K^+$ -W ion-atom potential

All calculations with the  $(KW)^+$  "molecular ion" have been performed in  $C_{\infty v}$  symmetry. Since  $(KW)^+$  is an open-shell system, the calculations were spin unrestricted. Binding energies have been calculated with respect to the energies of the W atom and the  $K^+$  ion in their experimental ground states. The tungsten experimental ground state is a  $^5D$  state with configuration  $[Xe](4f)^{14}(5d)^4(6s)^2$ .<sup>17</sup> We performed frozen-core calculations with the  $5d$  and  $6s$  acting as valence shells. In order to obtain a  $^5D$  state, all electrons in the  $5d$  orbital must be spin polarized. The  $K^+$  ground state is given by the Ar noble-gas configuration. Here, our valence shells consisted of the (occupied)  $3s$ ,  $3p$ , and (virtual)  $4s$  orbitals.

Figure 1 shows the  $(KW)^+$  molecular-orbital (MO) interaction picture for  $K^+$ -W separation  $r=1.3$  Å. The tungsten  $5d$  and  $6s$  orbital energies are effectively lower here than in the isolated atom due to the external Coulomb field of the potassium ion. The  $K^+$   $3p\sigma$  level is stabilized by the interaction with the W  $5d\sigma$  into the  $2\sigma$  MO, whereas this interaction destabilizes the W  $5d\sigma$  level. However, the resulting  $3\sigma$  MO is stabilized due to additional interaction with the higher  $K^+$   $4s$  and W  $6s$  levels. Mixing between the  $K^+$   $4s$  and the W  $5d\sigma$  and  $6s$  levels further leads to the virtual  $4\sigma$  and  $5\sigma$  MO's. The  $K^+$   $3s$  level is stabilized by a weak interaction with the W  $5d\sigma$  into the  $1\sigma$  MO. In the  $\pi$  symmetry, the interaction picture is similar, although much simpler: The interaction between the  $K^+$   $3p\pi$  and W  $5d\pi$  levels stabilizes the first into the  $1\pi$  and destabilizes the latter into the  $2\pi$  MO. Note that the electrons in both  $2\pi$  and  $1\delta$  MO's are spin polarized.

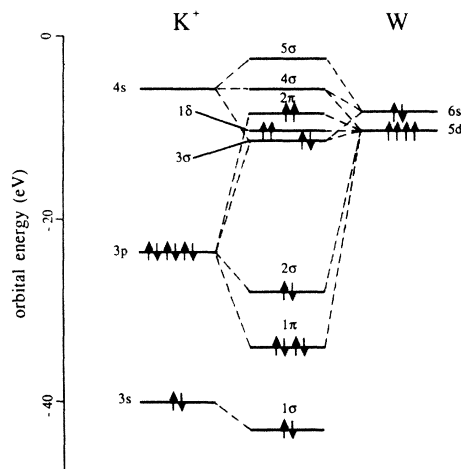


FIG. 1. MO-level picture of the  $(KW)^+$ -molecular ion for  $K^+$ -W separation 1.3 Å. The electronic configuration is  $(3\sigma)^2(2\pi)^2(1\delta)^2$ , where the  $2\pi$  and  $1\delta$  electrons are spin polarized.

If we go to shorter  $K^+$ -W distances,  $r < 1.3$  Å, the  $5d\pi$  orbital will be more and more destabilized due to stronger mixing with the  $3p\pi$ . Finally ( $r < 1.1$  Å), the energy gain from the spin polarization of the two  $2\pi$  electrons will be canceled by the  $1\delta \rightarrow 2\pi$  excitation energy and consequently the closed-shell  $(3\sigma)^2(1\delta)^4$  configuration will yield a lower  $K^+$ -W interaction energy than the spin-polarized  $(3\sigma)^2(2\pi)^2(1\delta)^2$  configuration.

For  $K^+$ -W separations  $r > 1.3$  Å, the W  $5d$  and  $6s$  levels mix less strongly with the  $K^+$   $4s$  level. Moreover, the  $5d$  and  $6s$  level energies will shift upwards towards the  $4s$  level energy. These two effects cause the  $3\sigma$ ,  $4\sigma$ , and  $5\sigma$  MO's to approach each other. Therefore, for  $r \geq 2$  Å, the excitation of one electron from the  $3\sigma$  to the  $4\sigma$  MO will be canceled by the energy gain due to additional spin polarization. The resulting molecular configuration, however, has the wrong dissociation limit for the tungsten atom [the  $(5d)^5(6s)^1$   $^7S$  state]. Moreover, it is generally known that the  $X\alpha$  potential tends to favor spin polarization too much (using LSD potentials<sup>18</sup> yielded similar results). Therefore, we did not consider the spin-polarized  $(3\sigma)^1(4\sigma)^1$  configuration in more detail, but instead retained also at larger  $K^+$ -W distances the  $(KW)^+$  molecular configuration depicted in Fig. 1, which has the same spin polarization as the W atom (the  $K^+$  spin polarization is zero).

For  $K^+$ -W separations  $r \geq 6$  Å, the  $K^+$   $4s$  and W  $6s$  and  $5d\sigma$  levels nearly become degenerate. Consequently, the molecular ground state will be a mixture of several configurations rather than consist of only one. Therefore, configuration-interaction (CI) calculations should be performed for the potential curve corresponding to the ground state of  $(KW)^+$  between 6 and 25 Å. For distances  $r > 25$  Å, the  $(KW)^+$  molecular ground state with the tungsten spin polarization corresponds to the  $(5d)^4(6s)^2$  configuration of the tungsten atom.

Figure 2 shows the calculated (HFS)  $K^+$ -W potential on a logarithmic (high-energy part) and a linear (low-energy part: inset) scale. From the above discussions, it is

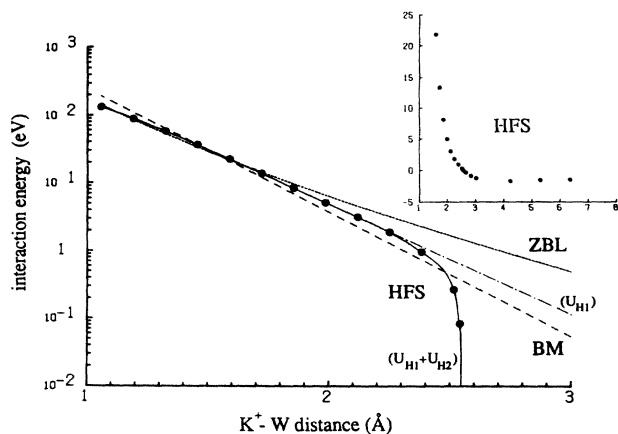


FIG. 2. High-energy part of the calculated  $K^+$ -W potential. The dot-dashed line indicates the extrapolated exponential HFS potential  $U_{H1}$  (see text). The potential is compared with the Born-Mayer potential of Tenner *et al.* ("BM," long-dashed line) and the ZBL universal potential ("ZBL," short-dashed line). Inset: low-energy part of the calculated  $K^+$ -W potential.

clear that we cannot trust the calculated points for  $K^+$ -W separations  $\geq 5$  Å; the agreement of the well depth with the experimental value of Hurkmans *et al.*<sup>5</sup> is therefore merely fortuitous. For the present discussion, however, we are only interested in the repulsive part of the calculated  $K^+$ -W potential between about 1 and 2.5 Å (see discussion below). In Fig. 2, the HFS  $K^+$ -W potential is compared with the best-fit Born-Mayer potential of Tenner *et al.*<sup>3,4</sup> and with the ZBL "universal" potential.<sup>7</sup> For  $1 < r < 2.3$  Å, we see that the agreement is generally quite good; especially at shorter distances there is excellent agreement between HFS and ZBL potentials. For  $r > 2.3$  Å, the HFS potential bends down to the chemical bond minimum. The Tenner BM potential is somewhat steeper than the HFS potential, whereas the ZBL potential has a larger tail.

We may write the HFS potential  $U_{HFS}(r)$  as the sum of two terms

$$U_{HFS}(r) = U_{H1}(r) + U_{H2}(r), \quad (4a)$$

where  $U_{H1}(r)$  represents the repulsive part of  $U_{HFS}(r)$  and  $U_{H2}(r)$  its attractive part (compare with Morse potential). From Fig. 2 we can see that, except for short distances, we may assume for  $U_{H1}(r)$  an exponential behavior,

$$U_{H1}(r) \approx 7771e^{-3.71r(\text{Å})} \text{ eV}. \quad (4b)$$

Now, for the present discussion we are mainly interested in the repulsive part of the ion-surface potential (and therefore, ion-atom potential), since it is this part which is predominantly probed by the experiments of Tenner *et al.* Moreover, we do not expect the attractive part of the  $K^+$ -W(110) potential to be a superposition of pairwise attractive  $K^+$ -W potentials. Therefore, we decided only to consider the repulsive part  $U_{H1}(r)$ . In Fig. 2 this means that for very low positive energies the HFS potential will be described by the dot-dashed line ( $U_{H1}$ ) rather than by

the (bent-down) solid line ( $U_{H1} + U_{H2}$ ).

In order to test the validity of a  $[Xe](4f)^{14}$  core for tungsten, we also calculated a potential curve with the 5s, 6s, 5p, 5d, and 4f as valence orbitals. Except for the very short distances ( $\leq 1$  Å), where core-core repulsion becomes non-negligible, this curve shows hardly any difference with the one shown in Fig. 2.

## B. Classical-trajectory calculations

Tenner *et al.*<sup>2,3</sup> measured the intensity  $I(E', \theta, \phi)$  of backscattered  $K^+$  ions as a function of backscattering energy  $E'$ , polar angle  $\theta$ , and azimuthal angle  $\phi$  (Fig. 3). In this subsection we will compare the  $I(E', \theta, \phi = 90^\circ)$  spectra resulting from classical-trajectory calculations using the HFS  $K^+$ -W ion-atom potential ( $S=1$ ) with experiment and with the spectra obtained from simulations with the Born-Mayer potential of Tenner *et al.*<sup>4</sup> ( $S=12$ ) and with the ZBL universal potential<sup>7</sup> ( $S=1$ ). We chose the value  $\phi = 90^\circ$  since in this direction the intensity spectra are most sensitive to the different choices of the pair potentials;<sup>3,4</sup> for other values of  $\phi$ , results turned out to show the same qualitative behavior. For reasons that will be discussed in Sec. III C, trajectory calculations were performed using the best-fit image potential of Tenner *et al.* [Eq. (1c)] with  $z_0 = -0.65$  Å and  $z_m = 1.5$  Å instead of a calculated attractive ion-surface interaction.

Figure 4 compares the simulated spectra obtained using different potentials with experiment for incident  $K^+$  energy  $E_0 = 35$  eV. Tenner *et al.*<sup>3,4</sup> distinguished three main types of peaks in the scattered  $K^+$  intensity [Fig. 4(a)], depending on the impact parameter of the incoming  $K^+$  ion. From their analysis it turned out that peaks B and A result from "near top-site" and "near hollow-site" impact parameters, respectively (Fig. 5). Peak C, resulting from "zig-zag" collisions,<sup>4</sup> probes a part of the unit cell somewhere halfway top site and hollow site. Now, if we compare the simulations using the  $S=1$  HFS potential with experiment, we see that peak B is clearly reproduced in the right position [Fig. 6(c)]. Peak A, on the contrary, is hardly present whereas peak C is present at a too small  $\theta$  value. Especially the near absence of peak A and the tendency of scattered  $K^+$  energies towards low values indicates an incorrect representation of the ion-surface potential at the hollow site. The  $S=12$  Born-Mayer potential of Tenner *et al.* gives a better representation of the hollow-site potential, which is clearly seen in Fig. 4(b).

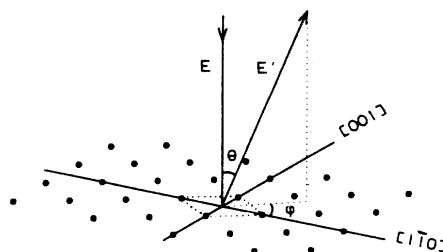


FIG. 3. Geometry of the W(110) surface and the  $K^+$  beam; the surface unit cell is indicated (dots). Figure taken from second paper of Ref. 3.

Note that in this spectrum, the  $\theta$  value of peak *B* is too large. This is due to the fact that the Tenner Born-Mayer potential falls off too steeply (see also Fig. 2). But, of course, we do not expect this potential to give an optimal reproduction of peak *B*, since its parameters have been determined with equal weights on the (nontop-site) peaks

*A* and *C*. If the tail of the potential is too large, as is the case for the ZBL potential (Fig. 2), peak *B* shifts towards a too small  $\theta$  value [Fig. 4(d)]. The ZBL potential hardly reproduces any structure that could be associated with a peak-type *A*.

In Fig. 6 contour plots of the scattered  $K^+$ -ion intensi-

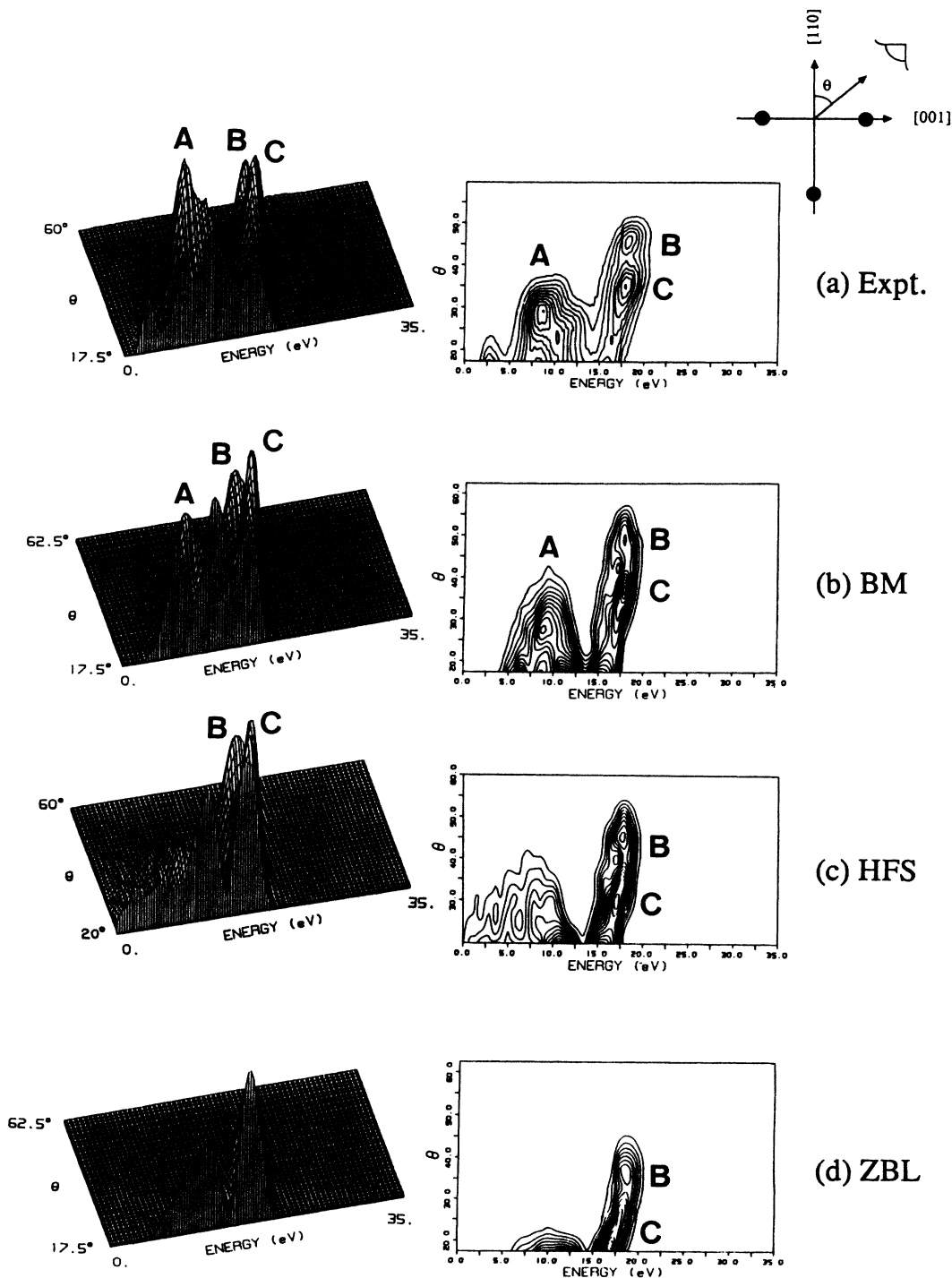


FIG. 4. Three-dimensional (left) and contour (right) plots of the intensity  $I(E', \theta, \phi)$  of  $K^+$  scattered from a W(110) surface for  $\phi = 90^\circ$  (Fig. 3, normal incidence,  $E_0 = 35$  eV). The experimental spectrum (a) is compared with simulated spectra for a number of potentials: The  $S=12$  best-fit Born-Mayer potential of Tenner *et al.* (b), the  $S=1$  HFS potential (c), and the  $S=1$  ZBL universal potential (d). The experimental data are from Ref. 3. The simulated spectra have been corrected for the experimental apparatus function. In the contour plots, the contour spacing is in arbitrary units (chosen for display purposes only).

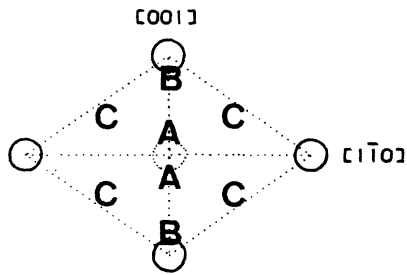


FIG. 5. Top view of the W(110) surface unit cell. The regions of impact parameters for the different types of peaks (*A, B, C*) are indicated.

ties are depicted for incident energies  $E_0=12$  eV and  $E_0=60$  eV. Roughly, we can see the same features as in the case of  $E_0=35$  eV: The HFS potential reproduces peak *B* at a somewhat better position in comparison with experiment than the Tenner Born-Mayer potential. The latter gives a better reproduction of the peak-*C* position. For  $E_0=12$  eV, both potentials overestimate the  $\theta$  value for peaks *B* and *C*. For  $E_0=60$  eV, both potentials cannot reproduce the complex peak-*A* structure very well.

From the above discussions, we may conclude that a sum of pairwise HFS  $K^+$ -W potentials gives a good approximation of the ion-surface potential for hyperthermal  $K^+$  scattering from the W(110) top sites (peak *B*); this in contrast to the universal ZBL potential which, due to its relatively large repulsion at lower energies, predicts too

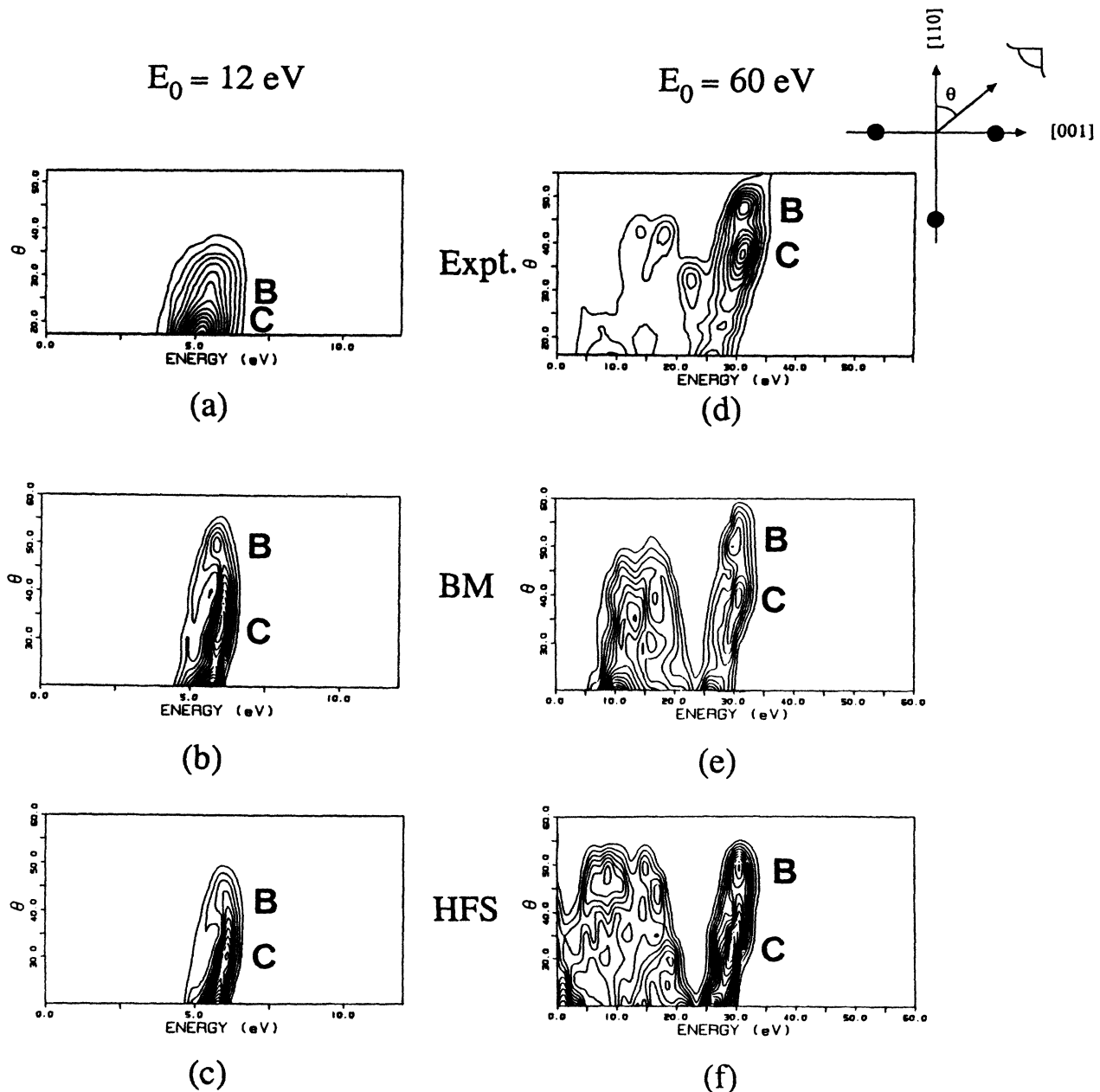


FIG. 6. Contour plots of scattered  $K^+$  intensities for incident energies  $E_0=12$  eV [(a)–(c)] and  $E_0=60$  eV [(d)–(f)]. See Fig. 4 for further explanation.

small backscattering angles  $\theta$  (Figs. 4 and 6).

As for  $K^+$  scattering from the  $W(110)$  hollow sites, it is clear that (the hollow-site) peak *A* cannot be reproduced using a purely pairwise additive ion-surface potential. The extra hollow-site repulsion with respect to a sum of pair potentials suggested by Hulpke and Mann<sup>6</sup> and Tenner *et al.*,<sup>3,4</sup> has already been briefly discussed in Sec. I. Hulpke and Tenner introduced this repulsion in order to get a reasonable fit to their experimental data. We tried to see if we could reproduce this repulsion by calculations from first principles. In order to do so, we first calculated the ion-surface (-cluster) potentials for a  $K^+$  ion approaching on the hollow site and on the top site of the surface unit cell (Sec. III C). Next, we compared these potentials with the sums of HFS pair potentials (Sec. III D). Finally, we tried to explain the extra hollow-site repulsion (Sec. III E).

### C. $K^+$ - $W_5$ ion-cluster potentials

The  $K^+$ - $W_5$  potential for a  $K^+$  approaching on the hollow site of the surface unit cell has been calculated using a (4,1)  $W_5$  cluster [Fig. 7(a)], whereas the top-site  $K^+$ - $W_5$  potential (which is not sensitive to second-layer atoms) has been determined using a (5,0) cluster [Fig. 7(b)]. The cluster structures have not been optimized, but taken from the bulk tungsten bcc crystal structure with a lattice constant of 3.16 Å. Note that the (4,1) cluster corresponds to the  $W(110)$  surface unit cell. The (4,1) and (5,0) clusters have  $C_{2v}$  and  $D_{2h}$  symmetry, respectively, although the

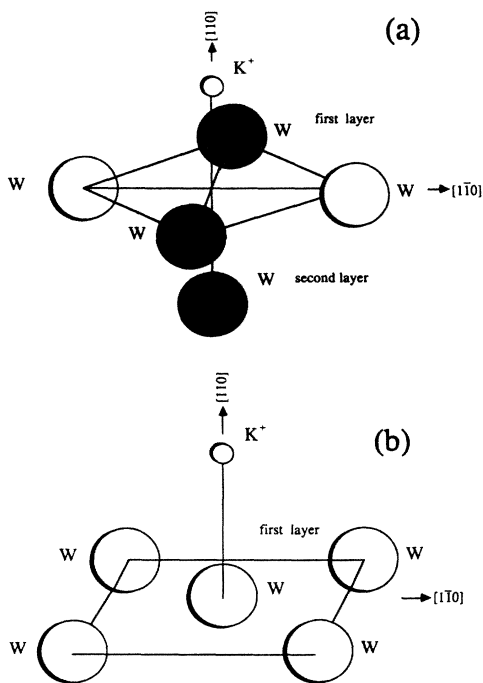


FIG. 7. Geometries of the  $W_5$  clusters used in the calculations of the  $K^+$ - $W_5$  potentials for a  $K^+$  ion approaching on the hollow site (a) and on the top site (b) of the  $W(110)$  surface unit cell. The shaded tungsten atoms in (a) lie in the  $(1\bar{1}0)$  plane; they are also depicted in Figs. 9(b) and 9(d). The atom sizes have been chosen arbitrarily.

symmetry of the  $K^+$ - $W_5(5,0)$  system is  $C_{2v}$ . Since  $(KW_5)^+$  is a closed-shell system, all ion-cluster calculations were spin restricted. The (4,1)-cluster ground-state configuration,

$$(6a_1)^2(2a_2)^2(4b_1)^2(3b_2)^2,$$

is determined unambiguously according to the Aufbau principle. As for the ground-state configuration of the (5,0) cluster, there are three competing levels:  $1a_u$ ,  $2b_{2u}$ , and  $4b_{3u}$ , over which two electrons have to be divided. It turns out, however, that the (5,0)-cluster ground-state energy is hardly dependent on which of the three levels is filled. We chose the

$$(4a_g)^2(1b_{1g})^2(2b_{2g})^2(1b_{3g})^2(1a_u)^2(2b_{1u})^2(1b_{2u})^2(3b_{3u})^2$$

as ground-state configuration ( $1a_u$  level filled). The ground-state configuration of the  $(KW_5)^+(4,1)$  (hollow-site) molecular ion is given by

$$(8a_1)^2(2a_2)^2(5b_1)^2(4b_2)^2$$

for  $z > 1.6$  Å and by

$$(8a_1)^2(2a_2)^2(4b_1)^2(5b_2)^2$$

for  $z \leq 1.6$  Å, although the energy difference between the two states is very small. For the  $(KW_5)^+(5,0)$  (top-site) molecular ion, there is the same ambiguity in defining the ground-state configuration as in the  $W_5(5,0)$  cluster case; we chose the

$$(8a_1)^2(2a_2)^2(6b_1)^2(3b_2)^2$$

configuration.

Figure 8 shows the calculated  $K^+$ - $W_5$  potentials for the  $K^+$  approaching on the top site (a) and on the hollow site (b) of the surface unit cell. In order to study the effect of image charge formation, we also calculated the potential energy for the  $K^+$  ion and a  $W_5^-(4,1)$  "ionic" cluster. If the  $K^+$  is very close to the surface, we may assume the image charge to be localized within the (4,1) cluster. Therefore, the total  $K^+$ - $W(110)$  potential (image potential included) for short distances may be better described by a  $K^+$ - $W_5^-$  potential than by the sum of a (repulsive)  $K^+$ - $W_5$  potential and the image potential  $V_{im}$  given by Eq. (1c). The latter sum, however, gives a better description of the  $K^+$ - $W(110)$  interaction far away from the surface, and it is not clear how the transition from a  $K^+$ - $W_5^-$  potential to the sum of a  $K^+$ - $W_5$  potential and  $V_{im}$  [Eq. (1c)] should be made when going to larger  $z$  values. For  $-0.5 \leq z \leq 5$  Å we calculated a  $K^+$ - $W_5^-$  potential curve which was about 3.5 eV lower in energy than the  $K^+$ - $W_5$  potential. Thus, even at larger distances, the  $K^+$ - $W_5^-$  curve remains below the  $K^+$ - $W_5$  curve, clearly reflecting its poor description of the total  $K^+$ - $W(110)$  potential far away from the surface. From this we conclude that we are unable to calculate image charge effects within our cluster approximation. Therefore, we had to rely on the "experimental" [Ref. 4, Eq. (1c)] image potential in our trajectory calculations (see Sec. III B). Since, however, for  $K^+$  incident energies between 10 and 100 eV mainly the repul-

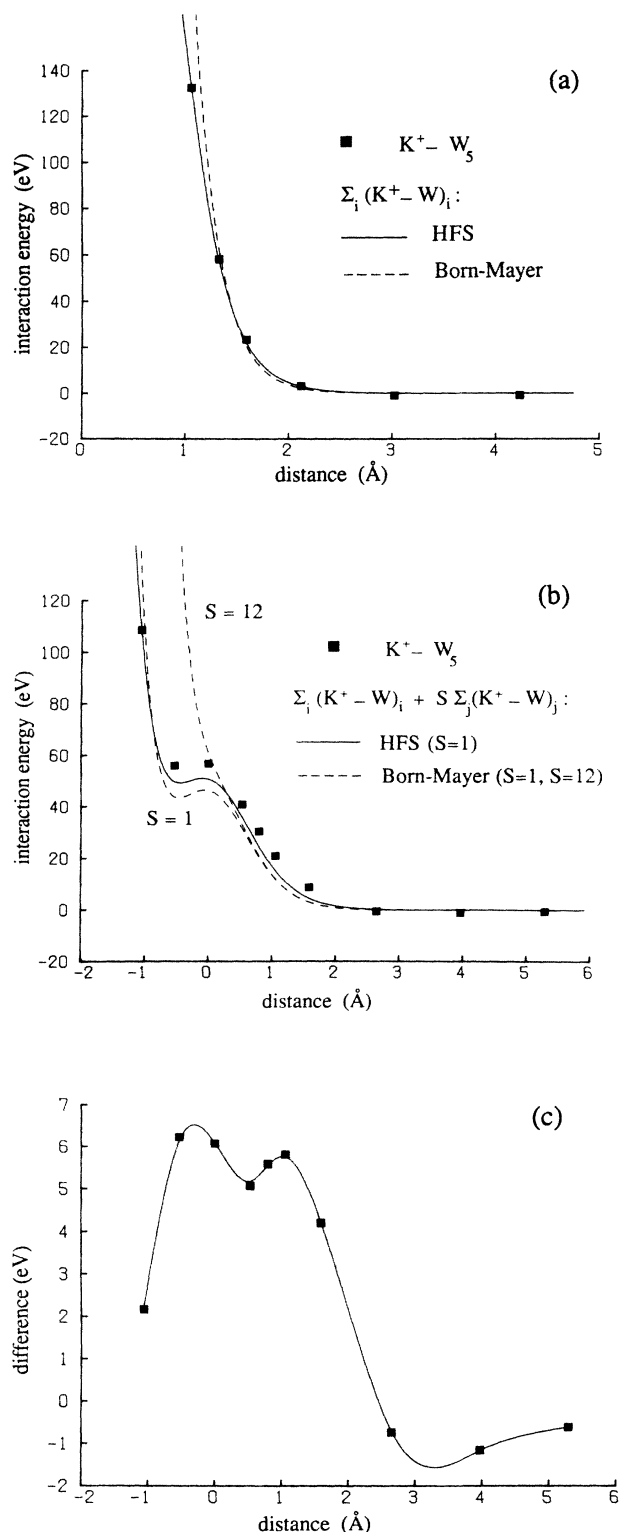


FIG. 8. Calculated  $K^+-W_5$  potentials for a  $K^+$  approaching on the top site (a) and on the hollow site (b) of the surface unit cell. The ion-cluster potentials are compared with the sums of HFS and Tenner BM pair potentials; these sums range over the tungsten atoms of the top-site cluster (a) and the hollow-site cluster (b). For the hollow site, the difference between the ion-cluster potential and the sum of HFS pair potentials is indicated (c).

sive wall of the ion-surface potential is probed, the simulated spectra do not depend very much on the attractive part.<sup>4</sup>

#### D. Breakdown of a summation of pair potentials

In Fig. 8, the  $K^+-W_5$  potentials are compared with the sums of pairwise HFS and Tenner BM (Ref. 4) potentials. The sums range over the tungsten atoms of the clusters. From Fig. 8(a), we see that the ion-cluster potential for a  $K^+$  ion approaching on the top site of the surface unit cell can be well approximated by a sum of pair potentials, as is, of course, to be expected. For the hollow-site  $K^+-W_5$  potential, however, there is a clear breakdown of the pairwise approximation, as we can see from Fig. 8(b). The  $K^+-W_5$  potential for a  $K^+$  ion at the center of the W(110) surface unit cell is about 6 eV more repulsive than the sum of pairwise HFS  $K^+-W$  potentials [Fig. 8(c)]. The  $S=12$  Tenner BM potential partly accounts for extra hollow-site repulsion, as is clear from Fig. 8(b). At higher energies, however, it overestimates the contribution from second-layer atoms. This can also be concluded from Fig. 6 for  $E_0=60$  eV, where the peak-A structure occurs at too high backscattering energy values.

Summarizing, Figs. 8(b) and 8(c) show that the calculated  $K^+-W(110)$  potential is characterized by an extra repulsion with respect to a superposition of pair potentials at the hollow site of the W(110) surface unit cell; this is in agreement with experimental work.<sup>3,4,6</sup> Section III E will describe which mechanisms can lead to such an extra repulsion.

#### E. Why extra hollow-site repulsion?

##### 1. Introduction

One might be tempted to explain extra hollow-site repulsion by assuming an electron charge-density enhancement at the center of the W(110) surface unit cell with respect to the sum of tungsten atomic charge densities. Instead, we calculated a small depletion [with respect to the  $(5d)^4(6s)^2$  W reference atoms]. Therefore, in order to explain extra repulsion, we have to look in more detail into what exactly happens to the electrons when we “push” the  $K^+$  ion into the W(110) hollow site; this is depicted in Fig. 9(d). This figure shows a contour plot in the  $(1\bar{1}0)$  plane of the change  $\Delta\rho$  in the electron charge density as a consequence of pushing the  $K^+$  ion into the hollow site [distance 0 in Fig. 8(b)] of the W(110) surface unit cell; the three tungsten atoms depicted are the shaded ones of the  $W_5(4,1)$  cluster in Fig. 7(a). More specifically,  $\Delta\rho = \rho_{\text{SCF}}(K^+W_5) - \rho_{\text{SCF}}(W_5) - \rho_{\text{SCF}}(K^+)$ , i.e., the difference between the SCF electron charge density of the  $K^+-W_5$  system and the SCF densities of the  $K^+$  ion and  $W_5$  cluster. A similar change  $\Delta\rho$  in the electron charge density as a consequence of putting together a W atom and a  $K^+$  ion is depicted in Fig. 9(c). If we take a closer look at Fig. 9(d), we see that due to the  $K^+$  interaction with the W(110) surface ( $W_5$  cluster) at the hollow site, electrons move away from certain areas in space ( $\Delta\rho < 0$ , dashed contours) to other areas ( $\Delta\rho > 0$ , solid contours). Now, we would expect a net move of electrons towards the  $K^+$  ion

due to its positive charge (this effect is, for example, clearly seen when a proton is embedded in jellium<sup>19</sup>). Figure 9(d), however, suggests the reverse: Electrons mainly *move away* from the  $K^+$  ion. This effect is, as we shall see, caused by *exchange repulsion* between the  $K^+$  ion and the  $W(110)$  surface ( $W_5$  cluster). By studying the effects of exchange repulsion, we have been able to indicate which mechanisms can cause the hollow-site  $K^+$ - $W(110)$  ion-surface potential to be more repulsive than the sum of pairwise  $K^+$ - $W$  ion-atom potentials. In Sec. III E 2 we will explain the main features of exchange repulsion; fi-

nally in Sec. III E 3 reasons are given for a breakdown of the pairwise approximation.

## 2. Exchange repulsion: General

The repulsive parts of the  $K^+$ - $W$  and  $K^+$ - $W(110)$  potentials for energies up to about 50 keV are mainly determined by exchange (Pauli, Born) repulsion. The role of exchange repulsion in the chemical bond has been studied by many authors (see, e.g., Ref. 9). The mechanism of exchange repulsion becomes clear by the following simple

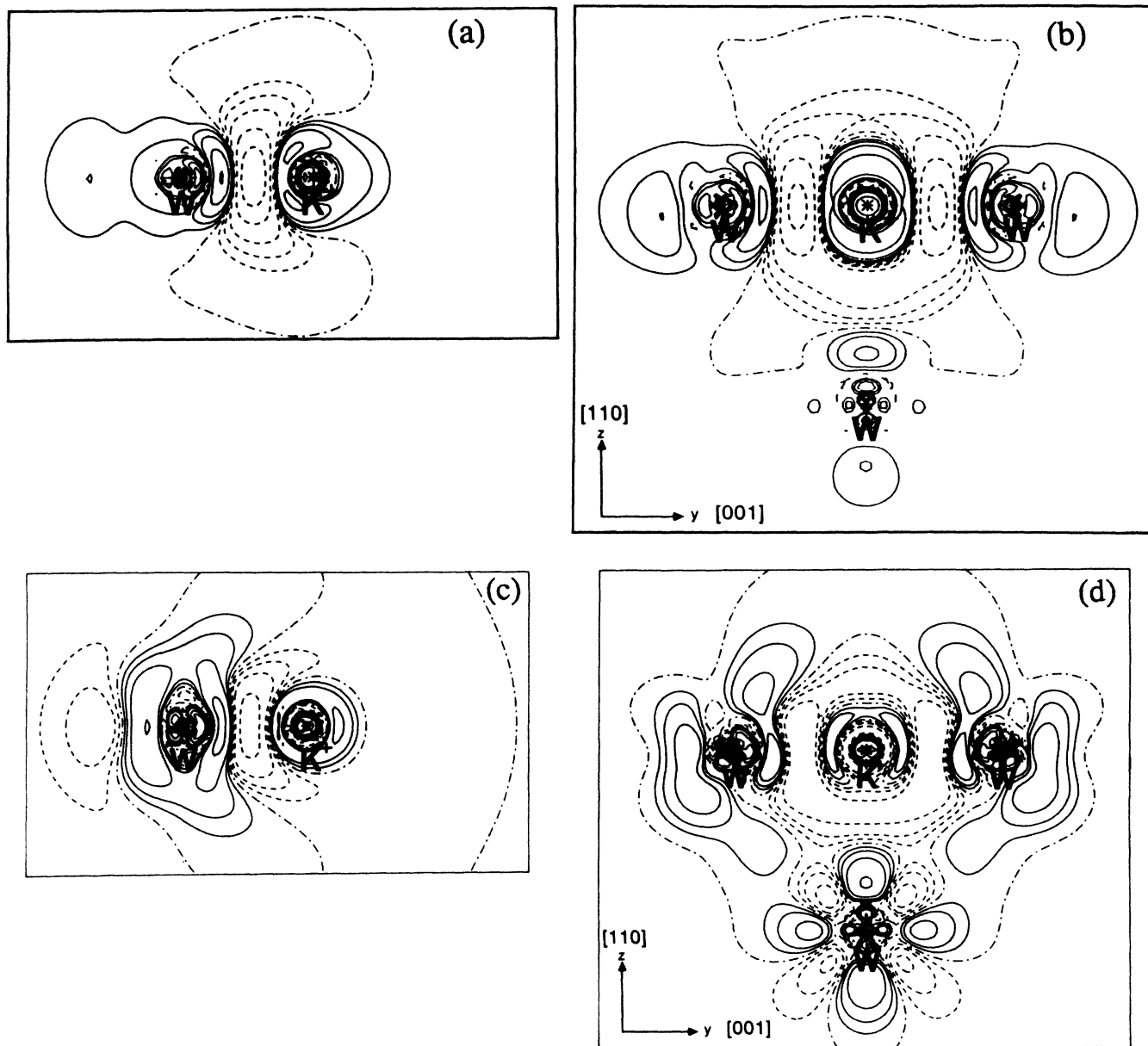


FIG. 9. Contour plots of the change  $\Delta\rho$  in electron charge density due to the  $K^+$ - $W$  ion-atom [(a) and (c)] and  $K^+$ - $W_5$  hollow-site ion-cluster [(b) and (d)] interactions. In (b) and (d), the electron charge rearrangement is plotted in the  $(1\bar{1}0)$  plane of the hollow-site cluster [Fig. 7(a)] for a  $K^+$  ion at the center of the  $W(110)$  surface unit cell [distance 0 in Fig. 8(b)]; the three plotted  $W$  atoms are the shaded ones of Fig. 7(a). Electronic charge rearrangements are plotted as a consequence of exchange repulsion alone [(a) and (b)] and of the combination of exchange repulsion and polarization-charge transfer [(c) and (d)]. Solid contours indicate  $\Delta\rho > 0$ , dashed contours  $\Delta\rho < 0$ , and dot-dashed contours  $\Delta\rho = 0$ . Contours drawn are  $\Delta\rho = 0, \pm 0.005, \pm 0.01, \pm 0.02, \pm 0.05, \pm 0.1, \pm 0.2$ , and  $\pm 0.5e/a_0^3$ . See text (Sec. III E) for further explanation.

example. If we put two atoms  $A$  and  $B$  together without allowing the occupied atomic orbitals  $\phi_A$  and  $\phi_B$  to mix with virtual (unoccupied) orbitals, the resulting charge density  $\rho_{AB}^0$  will nevertheless be different from the sum of atomic charge densities, that is,  $\rho_{AB}^0 \neq \rho_A + \rho_B$ . This is due to the requirement that the total electronic wave function of the system  $AB$  be antisymmetric,

$$\phi_{AB}(x, x') = \frac{1}{(1-S^2)^{1/2}} [\phi_A(x)\phi_B(x') - \phi_B(x)\phi_A(x')], \quad (5a)$$

where  $S = \langle \phi_A | \phi_B \rangle$ . The resulting one-electron charge density,

$$\begin{aligned} \rho_{AB}^0(x) &= \int |\phi_{AB}(x, x')|^2 dx' \\ &= \frac{1}{1-S^2} [|\phi_A(x)|^2 + |\phi_B(x)|^2 \\ &\quad - S\phi_A^*(x)\phi_B(x) - S\phi_A(x)\phi_B^*(x)], \end{aligned} \quad (5b)$$

indicates a relative *increase* in electron charge around the atomic cores of  $A$  and  $B$ , and a *decrease* in the interatomic region, where there is maximum overlap. The change in electron density from  $\rho_A + \rho_B$  to  $\rho_{AB}^0$  corresponds to a repulsive interaction between the two atoms  $A$  and  $B$  which is called *exchange (Pauli, Born) repulsion*. As is illustrated in Table II for the  $(KW)^+$  system, the change  $\rho_A + \rho_B \rightarrow \rho_{AB}^0$  stabilizes the Coulomb terms in the energy of the system  $AB$ , but the larger increase in electronic *kinetic* energy causes a net repulsive interaction; this is generally true in the repulsive energy range under consideration. Figure 10(a) shows the orbital interaction picture of exchange repulsion. If we only allow the occupied, overlapping orbitals  $\phi_A$  and  $\phi_B$  to interact, the result is a stabilized [ $\phi'_A$  in Fig. 10(a)] and a destabilized [ $\phi'_B$  in Fig. 10(a)] orbital.  $\phi'_A$  and  $\phi'_B$  are orthogonal, and the density  $\rho_{AB}^0$  given by Eq. (5b) can be written simply as  $\rho_{AB}^0 = |\phi'_A|^2 + |\phi'_B|^2$ . The destabilized orbital may, in the case of strong exchange repulsion, be high above the Fermi level  $E_F$ . Now, if we allow the virtual orbitals  $\phi_A^v$  and  $\phi_B^v$  to mix in [Fig. 10(b)], the first consequence is a stabilization of the orbitals  $\phi'_A$  and  $\phi'_B$  into  $\phi''_A$  and  $\phi''_B$ , respectively. However, if the stabilized orbital  $\phi''_B$  is still

TABLE II. Decomposition of the  $K^+$ -W ion-atom exchange repulsions in electronic kinetic energy terms and in Coulomb terms. The electronic configuration of the W atom in these model calculations was  $[\text{Xe}(4f)^{14}(6s)^2(5d\pi)^4]$ , that is, closed shell.  $r$  is the distance between the  $K^+$  ion and the W atom. Note that at larger distances  $r$ , the "exchange repulsion" changes into a (Coulomb) attraction (overlap  $S$  goes to zero).

$r$ (Å)	Kinetic energy (eV)	Coulomb energy (eV)
1.06	635	-436
1.59	251	-211
2.24	66.7	-62.6
3.18	13.1	-14.4

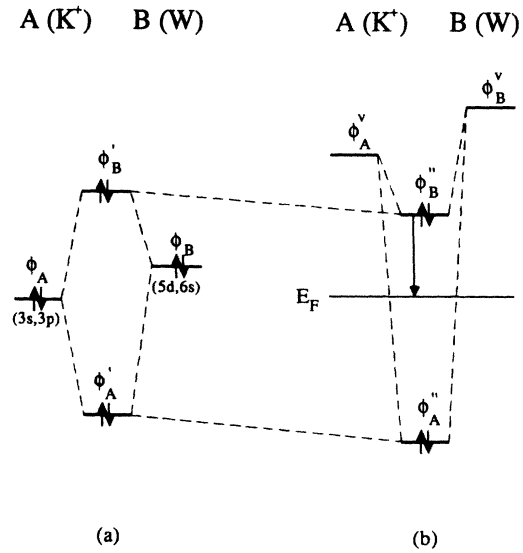


FIG. 10. Decomposition of the total interaction between atoms  $A$  and  $B$  into two parts: schematic orbital interaction picture of (i) exchange repulsion (a) and (ii) polarization-charge transfer (b); cf. Sec. III E 2.

above the Fermi level, an additional effect takes place: Deexcitation of the electrons from  $\phi''_B$  to the Fermi level. The combination of energy-level stabilization (due to mixing in of the virtual orbitals) and deexcitation to the Fermi level lowers the  $K^+$ -W(110) (or similarly,  $K^+$ -W) interaction energy; we call this *polarization-charge transfer*. Summarizing the above discussion, we may decompose the ion-surface (ion-atom) interaction energy into two parts; the first part is exchange repulsion which is a consequence of the antisymmetry requirement and can be obtained by only allowing the occupied ion and surface orbitals to mix [Fig. 10(a)]; the second part is the polarization-charge-transfer energy [Fig. 10(b)]. Thus, the net ion-surface (ion-atom) interaction energy is given by the sum of exchange repulsion and polarization-charge-transfer energy; this sum is *lower* than the exchange repulsion alone.

We now can examine (Fig. 9) how exchange repulsion and polarization-charge transfer affect the spatial distribution of electron charge. Figures 9(a) and 9(b) show the electron charge rearrangement  $\Delta\rho$  as a consequence of exchange *alone*; the geometries in Figs. 9(a) and 9(b) are the same as in Figs. 9(c) and 9(d), respectively. Now, recalling the discussion around Eq. (5b), we see that, indeed, electron charge is removed from regions where there is overlap between occupied atomic orbitals, i.e., from the interatomic regions. It is also qualitatively clear from Figs. 9(a) and 9(b) that the kinetic energy increases as a consequence of exchange. For a one-electron system described by a wave function  $\Psi$ , the kinetic energy  $E_{\text{kin}}$  equals

$$E_{\text{kin}} = -\frac{\hbar^2}{2m_e} \int \Psi^* \nabla^2 \Psi d\tau = \frac{\hbar^2}{2m_e} \int |\nabla \Psi|^2 d\tau,$$

and the gradient norm  $|\nabla\Psi|$  is coupled to the density ( $\rho = |\Psi|^2$ ) gradient via  $|\nabla\rho| = 2|\Psi||\nabla\Psi|$ . The effect of exchange is an increase of the charge-density gradient norm  $|\nabla\rho|$ , as we can see from Figs. 9(a) and 9(b), and therefore an increase in the electronic kinetic energy.

Figures 9(c) and 9(d) show the influence of the combination of exchange and polarization-charge transfer on the spatial distribution of electron charge; so, in going from Fig. 9(a) to Fig. 9(c) and from Fig. 9(b) to Fig. 9(d) we see the electrons rearranging themselves due to polarization-charge transfer. The main features of this rearrangement are in the first place a lowering of the density gradient norm; this is seen both if we go from Figs. 9(a)–9(c) and from Figs. 9(b)–9(d). The second feature, which is especially strong in the  $K^+W_5$  interaction [Figs. 9(b)–9(d)], is a removal of electrons from the region around the  $K^+$  ion. We can explain this feature with the aid of Fig. 10. The  $K^+W_5$  exchange repulsion pushes a part of the occupied  $K^+ 3s$  and  $3p$  orbitals far into the excited spectrum ( $\phi'_B$ ). Deexcitation of electrons from the stabilized orbital  $\phi''_B$  (still lying above the Fermi level) finally causes the partial  $3s/3p$  (and  $W 5d/6s$ ) depletion.

### 3. An explanation for extra repulsion

In this section we will use qualitative arguments, based on the knowledge from the previous two sections, to indicate two mechanisms which may contribute to an extra repulsion at the  $W(110)$  hollow site: (1) The *exchange repulsion* between the  $K^+$  ion and the cores of the surface  $W$  atoms is *larger* than the sum of pairwise  $K^+W$ -core exchange repulsions, and (2) the (absolute value of)  $K^+W_5$  polarization–charge-transfer energy may be *smaller* than the sum of pairwise  $K^+W$  polarization–charge-transfer energies due to a relative destabilization of its electrostatic part in the cluster.

TABLE III.  $K^+Er_2$  exchange repulsions  $\Delta E^0$  for a  $K^+$  ion placed in the middle between two  $Er$  atoms in comparison with the  $K^+Er$  exchange repulsion for the same  $K^+Er$  distance  $r$ . The electronic  $Er$  charge density in these model calculations was the same as that of the  $W$  core. The mutual overlap between the two  $Er$  atoms was neglected.

$r$ (Å)	$\Delta E^0$ (eV)	
	$K^+Er$	$Er-K^+Er$
0.79	254	579
1.06	145	324
1.32	68.6	146
1.59	27.2	56.5
2.24	1.91	3.84

As for (1), it is shown in the Appendix that if we put an atom  $A$  between two mutually nonoverlapping atoms  $B$ , the resulting exchange repulsion is larger than the sum of the two separate  $A-B$  exchange repulsions. This is also seen from Table III for a  $K^+$  ion placed in the middle between two “ $Er$ ” ( $Z=68$ ) atoms with the electronic charge density of the tungsten  $[Xe](4f)^{14}$  core; in these model calculations the  $Er$  atoms had no mutual overlap. From the Appendix and Table III we may conclude that the total exchange repulsion between the  $K^+$  ion and the five  $W$  cores in the cluster is indeed larger than the sum of pairwise  $K^+W$ -core exchange repulsions.

We can estimate the contribution from (2) by comparing Figs. 9(a) and 9(c) with 9(b) and 9(d). Note that the  $K^+W$  distance in Figs. 9(a) and 9(c) (1.58 Å) is the same as the distance between the  $K^+$  ion and the two first-layer  $W$  atoms in the Figs. 9(b) and 9(d). Now, the effect of polarization–charge transfer in the case of strong exchange repulsion is the partial depletion of electrons from

TABLE IV. Changes in the  $K^+$  and  $W/W_5$  gross populations (in electrons) due to the interaction between the  $K^+$  and  $W/W_5$  for a  $(KW)^+$  ion with  $K^+W$  distance  $r=1.58$  Å and a  $(KW_5)^+$  ion with the  $K^+$  ion at the center of the  $W(110)$  surface unit cell. Due to the large overlap of the diffuse  $K^+ 4s$  orbital with the diffuse  $W 6s$  and  $6p$  orbitals, the  $4s/6s/6p$  gross population changes in the table do not represent actual electron population changes in these orbitals, but rather in the interatomic region and around other atoms (for example, the 0.72 electron depletion from the “ $K^+ 4s$  orbital” for the  $K^+W_5$  case reflects the general trend of electron depletion from the overlapping regions around the  $K^+$  ion). The  $W 5d\sigma$  gross population of 0.68 electron in the  $(KW)^+$  molecular ion is due to a relief of  $K^+W$  exchange repulsion at larger distances ( $\sim 5$  Å) which effectively results in the transition of electron charge from the  $6s$  to the  $5d\sigma$  orbital.

	$K^+$			Other virtual orbitals	$W$	
	$3s$	$3p$	$4s$		$6s$	$6p$
$\sigma$	−0.03	−0.05	−0.11	0.68	−0.87	0.21
$\pi$		−0.05		0.08		0
$\delta$						

	$K^+$			Other virtual orbitals	$W_5$	
	$3s$	$3p$	$4s$		$\Sigma(\text{bcc})$	$\Sigma(\text{virt})$
$A_1$	−0.26	−0.12	−0.72	0.07	−2.31	3.35
$A_2$					−0.23	0.21
$B_1$		−0.10		0.04	−1.56	1.60
$B_2$		−0.64		0.28	−1.02	1.35

overlapping occupied orbitals, as we have seen earlier [cf. Fig. 10(b)]. If we compare the transitions from Fig. 9(a) to 9(c) and from Fig. 9(b) to 9(d), we see that there is much more electron depletion from the  $K^+$   $3s$  and  $3p$  orbitals in the cluster [Fig. 9(b)→9(d)] than in the diatomic [Fig. 9(a)→9(c)]. This is also clear from Table IV. This table shows that there is a large polarization-charge transfer from occupied  $K^+$  and  $W_5$  orbitals mainly to virtual  $W_5$  orbitals. The main effect of this, as is seen from Fig. 9(d), is an electron density enhancement at the “rear” of the  $W_5$  cluster, that is, far away from the overlapping regions, and therefore, from the  $K^+$  ion. Since the  $K^+$  is a positively charged ion, the greater electron depletion in the cluster may cause a relative destabilization of the (electrostatic part of the)  $K^+$ - $W_5$  interaction energy with respect to the  $K^+$ - $W$  pair interaction energy. This point is made clearer by the following. If we put a positive point charge  $+e$  at the position of the  $K^+$  ion and calculate the energy changes due to this point charge associated with the electron charge rearrangements corresponding to the transitions: Fig. 9(a)→9(c) and Fig. 9(b)→9(d), we obtain

$$\Delta \left\langle \frac{+e}{r} \right\rangle = \begin{cases} -2.7 \text{ eV } K^+-W \text{ [Fig. 9(a)→9(c)] ,} \\ +7.9 \text{ eV } K^+-W_5 \text{ [Fig. 9(b)→9(d)] .} \end{cases}$$

This means that polarization-charge transfer *lowers* the electrostatic energy due to a positive charge at the  $K^+$  site in the diatomic ( $K^+$ - $W$ ), whereas it *raises* this energy in the cluster, or in other words, causes extra (electrostatic) repulsion in the  $K^+$ - $W_5$  ion-cluster potential with respect to the  $K^+$ - $W$  ion-atom potential. Note that this effect may cause breakdown of a pairwise additive potential also in the case of a neutral adsorbate (instead of  $K^+$ ), but it will be stronger in the case of a positively charged ion.

#### F. Parametrization of extra repulsion

We might ask ourselves how we can incorporate extra hollow-site repulsion into a (parametrized) ion-surface potential which can be used in classical-trajectory calculations. If we assume the tungsten solid to consist of  $N$  atoms, the general problem is to find an (parametrized) approximation to the ion-surface potential

$$V(\mathbf{r}_{K^+}; \mathbf{R}_1, \mathbf{R}_2, \dots, \mathbf{R}_N) .$$

The “lowest-order” approximation to the  $(N+1)$ -body potential  $V$  is a sum of pairwise two-body potentials and a (one-body) image potential, i.e., Eq. (1) with  $S=1$ . A simple extension of this approximation incorporating extra hollow-site repulsion can be achieved by putting  $S>1$  in Eq. (1);<sup>3,4</sup> this has, however, the disadvantage that in  $K^+$  scattering from the W(110) hollow site the difference in momentum transfer to the solid due to extra hollow-site repulsion is completely put into the second-layer atoms, which is, of course, not very realistic. An alternative way of representing extra hollow-site repulsion is to add to Eq. (1) (with  $S=1$ ) an extra repulsive one-body potential depending only on the distance of the  $K^+$  ion above the surface;<sup>6</sup> however, this approach does not include any dependence of extra hollow-site repulsion on momentum transfer by the  $K^+$  ion to the surface tungsten atoms.

Clearly, the problem is that we cannot properly incorporate a repulsion which is centered *between* the surface atoms in an ion-surface potential which only consists of one- and two-body  $K^+$ -( $W$ ) ion-(atom) potentials. We therefore think that it might be fruitful to also include three-body potential terms into an approximation of the ion-surface potential  $V$ ; similar approximations are used in, e.g., molecular dynamics calculations.<sup>20</sup> Recently, this idea was also applied to thermal (helium) atom-surface scattering.<sup>21</sup>

#### IV. CONCLUSIONS

Using the HFS-LCAO method, we are able to calculate a  $K^+$ - $W$  ion-atom potential which yields, when used in classical-trajectory calculations, results that compare very well with experiment for hyperthermal  $K^+$  scattering from the W(110) top sites (where predominantly the pair potential between the  $K^+$  ion and a top  $W$  atom is probed). The “goodness” of the HFS  $K^+$ - $W$  potential is furthermore supported by the good agreement both between the top site  $K^+$ - $W_5$  ion-cluster potential and a sum of HFS pair potentials [Fig. 8(a)], and between the HFS and ZBL pair potentials at higher energies (Fig. 2), where the ZBL potential is expected to work better. A superposition of pairwise HFS  $K^+$ - $W$  potentials only fails to describe the  $K^+$  scattering from the hollow site of the W(110) surface unit cell. HFS-LCAO cluster calculations of the  $K^+$ -W(110) hollow-site potential show that this is due to the breakdown of a summation of pair potentials: The calculated hollow-site  $K^+$ -W(110) potential is more *repulsive* than a sum of pairwise  $K^+$ - $W$  potentials. This is in agreement with experimental observations.<sup>3,4,6</sup> Extra repulsion can be attributed to (1) an exchange repulsion between the potassium ion and the cores of the surface tungsten atoms, which is larger than the sum of pairwise  $K^+$ - $W$ -core exchange repulsions, and (2) the electrostatically destabilizing depletion of electrons from occupied overlapping  $K^+$  orbitals occurring in polarization-charge transfer as a consequence of strong exchange repulsion; this is hardly seen in the case of the  $(KW)^+$  diatomic. From the discussion in Sec. III E, it is clear that extra hollow-site repulsion cannot be explained from a hollow-site electron density which is larger than the sum of (tungsten) atomic electron densities. We therefore do not expect effective medium theory<sup>22</sup> to describe the ion-surface potential very well at hyperthermal energies. This is, of course, not very surprising since the interaction in this case takes place very near to the  $K^+$  and  $W$  atomic cores.

#### ACKNOWLEDGMENTS

The Free University is gratefully acknowledged for supplying financial support for the calculations. This work is part of the research program of the Netherlands Foundation for Fundamental Research on Matter (Stichting voor Fundamenteel Onderzoek der Materie) and was made possible by financial support from the Netherlands Organization for the Advancement of Pure Research (Nederlandse Organisatie voor Zuiver-Wetenschappelijk Onderzoek).

## APPENDIX

If we put together atoms  $A$  and  $B$  at some distance  $d$  without allowing the occupied orbitals  $\phi_A$  and  $\phi_B$  to mix with virtual orbitals, the antisymmetry requirement leads to kinetic exchange repulsion; this can be evaluated by calculating the total  $AB$  electronic kinetic energy

$$E_{\text{kin}}(AB) = \langle \phi_{AB} | (-\hbar^2/2m)(\nabla_x^2 + \nabla_{x'}^2) | \phi_{AB} \rangle,$$

where  $\phi_{AB}$  is given by Eq. (5a). If we orthogonalize  $\phi_A$  and  $\phi_B$  to each other,  $E_{\text{kin}}(AB)$  directly follows from Slater's rules. Let us orthogonalize  $\phi_A$  to  $\phi_B$ ; this yields  $\bar{\phi}_A = (1 - S^2)^{-1/2}(\phi_A - S\phi_B)$ , where  $S = \langle \phi_A | \phi_B \rangle$ , and

$$E_{\text{kin}}(AB) = T_{\bar{A}\bar{A}} + T_{BB} \\ \approx T_{AA} + T_{BB} + \frac{S^2}{1 - S^2}(T_{AA} + T_{BB}), \quad (\text{A1})$$

which indeed indicates a repulsive interaction. In Eq. (A1)

$$T_{AA} = \langle \phi_A | (-\hbar^2/2m)\nabla^2 | \phi_A \rangle,$$

etc. In the derivation of (A1) we approximated  $T_{AB} \approx 0$ . Now, if we put atom  $A$  in the middle between two atoms  $B$  described by wave functions  $\phi_{B_1}$  and  $\phi_{B_2}$  (the only

difference between these two wave functions is that they are centered around different points in space), we orthogonalize  $\phi_A$  to  $\phi_{B_1}$  and  $\phi_{B_2}$ . We put  $\langle \phi_{B_1} | \phi_{B_2} \rangle = 0$ ; furthermore, we retain the same  $A$ - $B$  distance  $d$  as described above, from which follows  $\langle \phi_A | \phi_{B_1} \rangle = \langle \phi_A | \phi_{B_2} \rangle = S$ . Orthogonalization of  $\phi_A$  to  $\phi_{B_1}$  and  $\phi_{B_2}$  leads to

$$\tilde{\phi}_A = \frac{1}{(1 - 2S^2)^{1/2}}(\phi_A - S\phi_{B_1} - S\phi_{B_2})$$

and

$$E_{\text{kin}}(BAB) = T_{\tilde{A}\tilde{A}} + T_{B_1B_1} + T_{B_2B_2} \\ \approx T_{AA} + 2T_{BB} + \frac{2S^2}{1 - 2S^2}(T_{AA} + T_{BB}), \quad (\text{A2})$$

where  $E_{\text{kin}}(BAB)$  is the total kinetic energy of the system  $BAB$ . If we compare Eqs. (A1) and (A2), we see that the extra repulsive term for  $BAB$  is larger than twice the repulsive term for  $AB$ , that is,

$$\frac{2S^2}{1 - 2S^2}(T_{AA} + T_{BB}) > 2 \frac{S^2}{1 - S^2}(T_{AA} + T_{BB}),$$

from which follows that in this case summation of pair potentials does not hold for the kinetic repulsion.

- <sup>1</sup>A. Boers, *Comments At. Mol. Phys.* **16**, 65 (1985); J. F. van der Veen, *Surf. Sci. Rep.* **5**, 199 (1985).  
<sup>2</sup>J. A. Barker and D. J. Auerbach, *Surf. Sci. Rep.* **4**, 1 (1985).  
<sup>3</sup>A. D. Tenner, K. T. Gillen, T. C. M. Horn, J. Los, and A. W. Kleyn, *Phys. Rev. Lett.* **52**, 2183 (1984); *Surf. Sci.* **172**, 90 (1986).  
<sup>4</sup>A. D. Tenner, R. P. Saxon, K. T. Gillen, D. E. Harrison, T. C. M. Horn, and A. W. Kleyn, *Surf. Sci.* **172**, 121 (1986).  
<sup>5</sup>A. Hurkmans, E. G. Overbosch, and J. Los, *Surf. Sci.* **62**, 621 (1977).  
<sup>6</sup>E. Hulpke and K. Mann, *Surf. Sci.* **133**, 171 (1983).  
<sup>7</sup>J. P. Biersack and J. F. Ziegler, *Nucl. Instrum. Methods* **194**, 93 (1982); J. F. Ziegler, J. P. Biersack, and U. Littmarck, in *The Stopping and Range of Ions in Solids*, Vol. 1 of *The Stopping and Ranges of Ions in Matter*, edited by J. F. Ziegler (Pergamon, New York, 1985); D. J. O'Connor and J. P. Biersack, *Nucl. Instrum. Methods B* **15**, 14 (1986).  
<sup>8</sup>S. H. Overbury and D. R. Huntley, *Phys. Rev. B* **32**, 6278 (1985).  
<sup>9</sup>D. Post and E. J. Baerends, *Surf. Sci.* **109**, 167 (1981); **116**, 177 (1982); D. Post and E. J. Baerends, *J. Chem. Phys.* **78**, 5663 (1983).  
<sup>10</sup>A. Olson and B. J. Garrison, *J. Chem. Phys.* **83**, 1392 (1985).  
<sup>11</sup>P. Nordlander, S. Holloway, and J. K. Nørskov, *Surf. Sci.*

**136**, 59 (1984).

- <sup>12</sup>H. Gollisch and L. Fritsche, *Surf. Sci.* **92**, 325 (1980).  
<sup>13</sup>E. J. Baerends, D. E. Ellis, and P. Ros, *Chem. Phys.* **2**, 41 (1973); E. J. Baerends and P. Ros, *ibid.* **2**, 52 (1973); **8**, 41 (1975).  
<sup>14</sup>P. M. Boerrigter, G. te Velde, and E. J. Baerends (unpublished).  
<sup>15</sup>J. G. Snijders, P. Vernooijs, and E. J. Baerends, *Atom. Data Nucl. Data Tables* **26**, 483 (1981); Internal Report [Free University, Amsterdam, 1981 (unpublished)].  
<sup>16</sup>T. Ziegler and A. Rauk, *Theor. Chim. Acta* **46**, 1 (1977).  
<sup>17</sup>C. E. Moore, *Natl. Bur. Stand. (U.S.) Circ. No. 467* (U.S. GPO, Washington, D.C., 1958), Vol. III.  
<sup>18</sup>O. Gunnarsson and B. I. Lundqvist, *Phys. Rev. B* **10**, 4274 (1976); S. H. Vosko, L. Wilk, and M. Nusair, *Can. J. Phys.* **58**, 1200 (1980).  
<sup>19</sup>B. I. Lundqvist, O. Gunnarsson, H. Hjelmberg, and J. K. Nørskov, *Surf. Sci.* **89**, 196 (1979).  
<sup>20</sup>J. N. Murrell, S. Carter, S. C. Farantos, P. Huxley, and A. J. C. Varandas, *Molecular Potential Energy Functions* (Wiley, New York, 1984).  
<sup>21</sup>P. W. Fowler and J. M. Hutson, *Phys. Rev. B* **33**, 3724 (1986).  
<sup>22</sup>N. Esbjerg and J. K. Nørskov, *Phys. Rev. Lett.* **45**, 807 (1980).

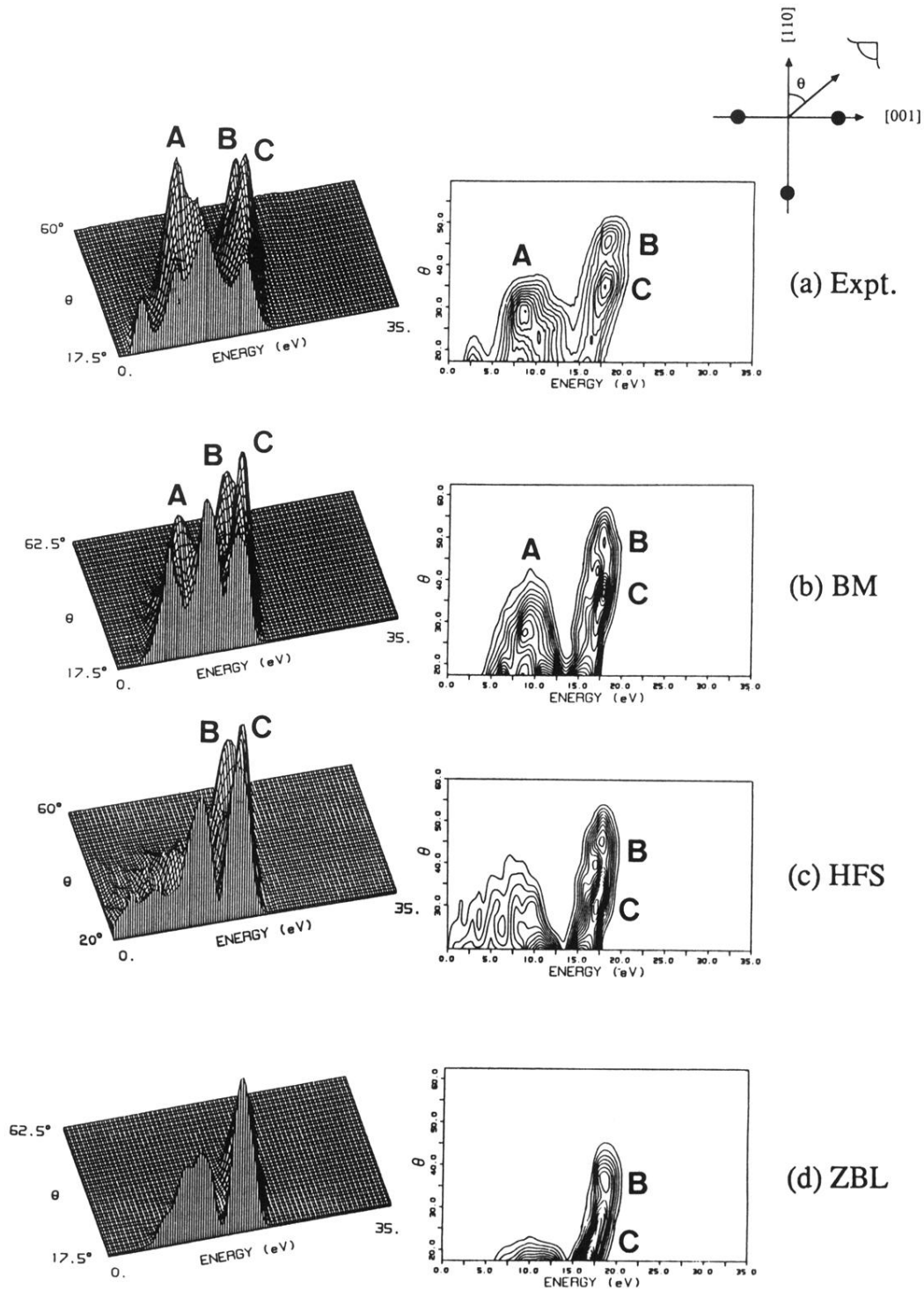


FIG. 4. Three-dimensional (left) and contour (right) plots of the intensity  $I(E', \theta, \phi)$  of  $K^+$  scattered from a W(110) surface for  $\phi = 90^\circ$  (Fig. 3, normal incidence,  $E_0 = 35$  eV). The experimental spectrum (a) is compared with simulated spectra for a number of potentials: The  $S=12$  best-fit Born-Mayer potential of Tenner *et al.* (b), the  $S=1$  HFS potential (c), and the  $S=1$  ZBL universal potential (d). The experimental data are from Ref. 3. The simulated spectra have been corrected for the experimental apparatus function. In the contour plots, the contour spacing is in arbitrary units (chosen for display purposes only).

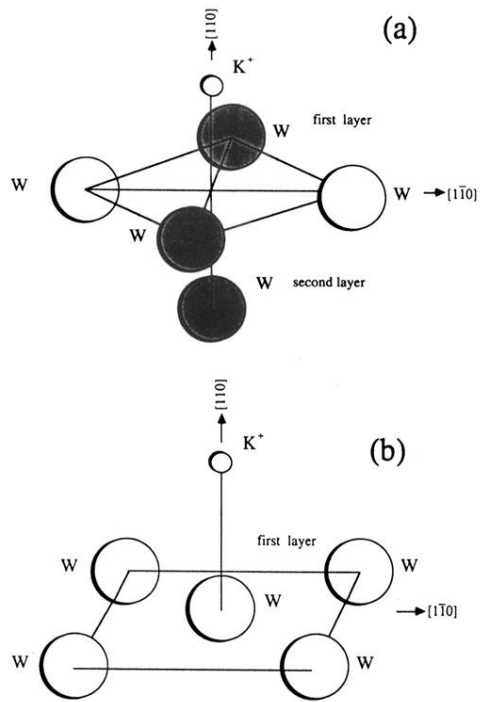


FIG. 7. Geometries of the  $W_5$  clusters used in the calculations of the  $K^+-W_5$  potentials for a  $K^+$  ion approaching on the hollow site (a) and on the top site (b) of the  $W(110)$  surface unit cell. The shaded tungsten atoms in (a) lie in the  $(1\bar{1}0)$  plane; they are also depicted in Figs. 9(b) and 9(d). The atom sizes have been chosen arbitrarily.